COMBINING A VIBRATION-BASED SHM-SCHEME AND AN AIRBORNE SOUND APPROACH FOR DAMAGE DETECTION ON WIND TURBINE ROTOR BLADES

Stavroula TSIAPOKI [1], Thomas KRAUSE [2], Moritz W. HÄCKELL [1], Raimund ROLFES [1], Jörn OSTERMANN [2]

[1] Institute of Structural Analysis, Leibniz Universität Hannover, Appelstraße 9a, Hanover 30167 GERMANY, s.tsiapoki@isd.uni-hannover.de, m.haeckell@isd.uni-hannover.de, r.rolfes@isd.uni-hannover.de
[2] Institut für Informationsverarbeitung, Leibniz Universität Hannover, Appelstraße 9a, Hanover 30167 GERMANY, krause@tnt.uni-hannover.de, ostermann@tnt.uni-hannover.de

Key words: wind turbine, rotor blades, SHM-scheme, vibration-based, acoustic emission, fatigue test.

Abstract

In the current work, a vibration-based SHM-scheme and an acoustic emission (AE) approach based on airborne sound are tested for damage detection at wind turbine rotor blades. The vibration-based approach includes the estimation of condition parameters (CPs), machine learning by means of data classification for changing environmental and operational conditions (EOCs) and hypothesis testing by using the acceleration signals of six measurement positions that are distributed over the blade length. A residue from the stochastic subspace identification (SSI) method and a residue from a vector autoregressive (VAR) model were used, in order to obtain two CPs. These are used as indicators for changes in the response of the structure. The airborne sound acoustic mission damage detection approach monitors the blade with three fiber optical microphones. A model of the cracking sound was developed, which describes characteristics of these sounds in the time-frequency-power domain. A detection algorithm uses these characteristics to detect damages, to estimate their significance and to handle environmental noise. Both methods were applied on data from a fatigue test of a 34 m rotor blade, which was harmonically excited for over one million load cycles in edgewise direction, leading to a significant damage at the trailing edge. Further, the potential of combining the two complementary approaches is investigated.

1 INTRODUCTION

Different SHM approaches have recently been applied on rotor blades for damage detection purposes. The majority of these are performed in smaller scales under laboratory conditions and only a few were tested in full scale or under operational conditions. The most commonly used SHM methods on rotor blades are acoustic emission (AE) [1], vibration-based methods [2] [3], strain measurement [4] and ultrasonic wave propagation [5]. Nevertheless, monitoring the blades of wind turbines in operation still poses many difficulties, so that visual inspections are often necessary for decisions concerning maintenance, repair and standstill. One of the principal reasons for this are the challenging and varying environmental and operational conditions (EOCs).

A modular SHM-scheme for monitoring engineering structures under varying EOCs and its application on different structures is presented in [6] [7] [8]. The framework includes three stages for both training and testing phases: machine learning, estimation of absolute and

reference-based condition parameters (CPs) and finally hypothesis testing based on probabilistic models. The application of this SHM framework on the fatigue test of a 34 m rotor blade is presented in [9]. Damage at the trailing edge as well as fatigue state was successfully detected. In the current paper, an additional CP based on the residue from Vector Autoregressive (VAR) models and the results for different confidence intervals are presented for the same experiment. Thus the applicability of different methods for the detection of structural changes at rotor blades is investigated and their results are compared.

In [10] [11] [12] a new acoustic emission (AE) approach was presented. The objective was to monitor the blade with a significantly lower amount of sensors compared to common AE approaches. Therefore the airborne sound in lower frequencies from about 550 Hz to 30 kHz was used. Only three fiber optical microphones were utilized for monitoring the whole blade. A model of the cracking sound and a real-time capable pattern recognition algorithm were developed. The algorithm detects the pattern of damages, estimates their significance and handles environmental noise, which is also present in these frequencies. In [9] the structural damage as well as parts of the crack increase were detected without false alarms. Very small damages could not be detected with the algorithm.

A potential increase of the damage detection performance is achieved by the combination of different monitoring approaches. Since different physical measurements are used, the combination of the vibration-based approach with the acoustic emission approach is beneficial. The vibration-based approach monitors continuously the condition of the system and detects changes, while the acoustic emission approach detects damage events almost instantly.

2 METHODOLOGY

2.1 SHM-Scheme and reference-based condition parameters

The SHM framework and its three constituent parts of machine learning, estimation of CPs and hypothesis testing are shown in Figure 1. First, data from different healthy system states are used for training. These are assigned to different data groups (clusters) depending on their EOCs. Then the CPs are calculated for each cluster. In the testing phase new incoming data sets are assigned to the existing clusters and their CPs are calculated. Finally, hypothesis testing is performed for different distributions of the CPs. For the investigated experiment the load level was considered a varying testing and excitation condition and was used for the classification of data sets. Here, two different classifications were conducted. In the first one (assigned as Man1 or Classification 1) all data sets were considered to belong to one cluster. In the second (Man2 or Classification 2) the data sets are grouped to clusters according to the applied load level.

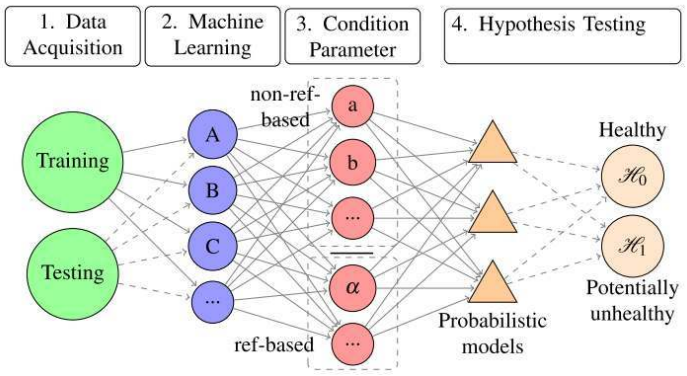

Figure 1: Modular SHM framework: Training and subsequently testing data instances are analyzed through a combination of a machine learning algorithm, condition parameters and probabilistic models.

Absolute and reference-based CPs can be estimated for SHM purposes directly from the measured time series in the context of the SHM-scheme used. Absolute CPs (i.e. modal parameters) can be calculated by single data sets. On the contrary, reference-based CPs are formed by residues, by comparing each data set with a reference from another data set and instance. In the case of data classification, each data set of a particular class is compared to a mean reference matrix in that class. In the current work, two reference-based CPs were used as indicators for structural changes. The first CP (CP^{γ}) is a residue based on the SSI approach, which is an alternative to the classical SSI residue [13] and is robust to changing excitation [14]. CP^{γ} depends on the number of blocks in the Hankel matrix, the number of significant values of the SVD matrices and the number of blocks the data set is divided into. The second CP (CP^{R^2}) is derived from a VAR model and is based on the coefficient of determination according to Neter [15]. A parameter that affects CP^{R^2} is the model order, which corresponds to the number of previous steps used for building the VAR model.

For hypothesis testing two probabilistic models were used. These affect the upper and lower control limits (UCL/LCL) of the control charts and thus the sensitivity of damage detection. The first one is based on a Gaussian distribution and the second one employs percentiles and is based on a discrete distribution. Receiver operating characteristic curves (ROCs) were used for the evaluation of the CPs' overall performance through a variation of the confidence interval.

2.2 AIBORNE SOUND DAMAGE DETECTION ALGORITHM

A real time capable damage detection algorithm which uses airborne sound signals is presented in [10]. The algorithm detects the audio pattern of damage sounds and estimates the damage significance. These cracking sounds are described by an impulse with a low raising time over a wide frequency range. Their power is logarithmically decreasing towards high frequencies from the frequency with maximal power and also decreasing over time. The damage detection algorithm uses features to represent these characteristics. The six features are based on the data of the power spectrum calculated by a windowed short-time Fourier transform. These features are listed as follows and are described in detail in [10] and [11].

- Power impulse feature: measures the signal power in a time period of 53.3 ms. It is also used as an indicator for the significance of a detected event.
- Power gradient feature: measures if the signal is impulse-like in a wide frequency range.
- Spectral flatness feature: measures if the signal is noise-like or tonal.
- Spectral slope feature: indicates a decrease in power towards high frequencies using linear regression.
- Spectral similarity feature: calculates the Euclidean distance to a linear model curve.
- Power slope feature: tests if the impulse power is decreasing over time.

The classifier is an and-combined comparison to threshold parameters. The principle flow chart of the algorithm is illustrated in Figure 2.

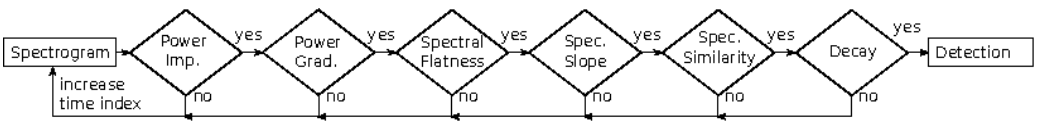

Figure 2. Principle flow-chart of the airborne sound damage detection algorithm.

3 FATIGUE TEST OF A WIND TURBINE ROTOR BLADE

A full scale fatigue test in edgewise direction was performed on a 34 m wind turbine rotor blade. The objective of the test was to introduce structural failure to the blade, while monitoring the structural responses continuously. Gradually increasing dynamic loads were applied by means of one load frame at a blade radius of 17 m for approximately 1.3 million cycles. The blade was excited close to the first edgewise eigenfrequency. In Figure 3 the sensor types that were used and their sensor positions are shown. For the vibration-based approach accelerometers and geophones were applied. The geophones and accelerometers were distributed along the blade both on the inside and outside of the blade. For positions P1 and P2 the velocity was derived, in order to obtain the acceleration, which was used in the performed analysis (see Figure 3). For the AE approach three fiber optical microphones were installed inside the blade on the webs. Two microphones were applied on the side of the trailing edge and the third one on the side of the leading edge.

The blade failed with a crack through the trailing edge at a blade radius of approximately 6 m from the root. In Table 1 the load steps, with the corresponding load levels and number of cycles are presented. The load levels refer to a reference point for load application, which was at a radius 2 m from the blade root. In addition, the accumulated damage at a radius 6 m from the blade root, where the significant damage occurred, is included as calculated by Minor's rule. Finally, the results of the visual inspections are shown. The blade condition can be divided into four states: undamaged state (steps 1-7), fatigue signs and insignificant damages (steps 8-10), occurence of trailing edge damage (step 11) and crack propagation (steps 12-17). The term insignificant damages refers to small delaminations and small material or bondline cracks.

Step	Load at 2 m	Estimated number of full cycles	Accumulated damage at 6 m	Results of visual inspection
1	70.0 %	94,012	0.0120	Undamaged state and 112 insignificant damages
2	75.6 %	327,098	0.1013	
3	81.1 %	94,817	0.1539	
4	90.0 %	95,632	0.3041	
5	95.6 %	103,644	0.5975	
6	105.0 %	45,900	0.9342	
7	110.0 %	277,733	4.1784	
8	120.0 %	70,069	6.1323	Fatigue signs and 95 insignificant damages
9	130.0 %	12,671	6.9189	
10	140.0 %	70,766	16.1375	
11a	170.0 %	1,874	16.1956	6 insignificant damages
11b	170.0 %	3,372	20.9004	Trailing edge damage of total length equal to 44 cm
12	50.0 %	3,912	20.9004	Damaged state/Crack propagation equal to 0.3 cm
13	70.0 %	4,256	20.9009	
14	90.0 %	1,895	20.9039	
15	105.0 %	10,094	20.9780	Damaged state/Crack propagation equal to 8.9 cm
16	115.0 %	4,002	21.0509	Damaged state/Crack propagation equal to 2.2 cm
17	130.0 %	4,285	21.3169	Damaged state/Crack propagation equal to 17.7 cm

Table 1: Load at section 2 m from blade root, number of cycles and accumulated damage at section 6 m from blade root and blade state.

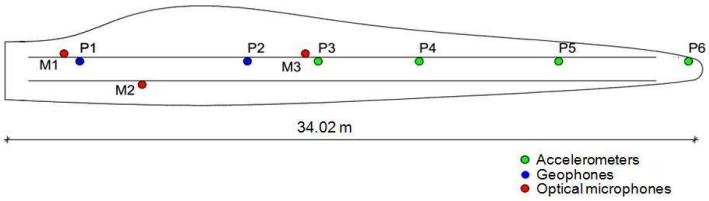

Figure 3: Sensor types and positions.

4 RESULTS

4.1 SHM-SCHEME

The analyzed database contained 1162 data sets, with 357 training and 810 testing data sets, each with duration of 10 minutes. In the training phase, only data sets from the healthy structure were used. In the testing phase, data sets from the damaged structure (fatigue and damage at trailing edge) as well as some healthy data sets were used. Thus, 50% of the data sets of steps 1 to 6 (see Table 1) and 34 data sets from the beginning of step 7 (load level 110%) were used for training and the remaining were used in the testing phase. The database was downsampled to 50 Hz for the analysis. The detection of the trailing edge damage and of structural changes due to fatigue were intended. Therefore, all the data sets of steps 8 to 17 (i.e. from 120%) were considered to be damaged. Acceleration occurring from sensors at positions 1 and 3 to 6 were included in the analysis for the estimation of the two CPs. The sensor in position P2 was excluded due to erroneous signals. Data normalization was performed, in order to minimize the effect of the applied load and vibration amplitude on the changes of the CPs. Thus, for the analysis the standard deviation of the signals of each position remained the same for all load levels. The references used for forming the two CPs were obtained as the mean values of the corresponding matrices of all the training data sets contained in a cluster. For every 10-minute data set, one CP was calculated.

In Figures 4 and 5 the control charts and the ROC curves are presented for SSI robust CP (CP^{γ}) and for the R^2 VAR-CP (CP^{R^2}). The control chart has been divided into two plots, (a) and (b), so that the results can be better discerned. The normalized values of the CPs for both discrete (CP_D^{γ}) and Gaussian distribution (CP_G^{γ}) are presented with light blue and dark blue lines respectively. The grey area indicates the damaged data sets. The ROC curves in Figure 4(c) and 5(c) provide an overview of the overall performance of the CPs and a comparison between Classifications 1 and 2 (Man1 and Man2) as well as the assumption for discrete or Gaussian distribution. Performance lines with ratio equal to 10:1, 3:1, 2:1 and 1:1 are shown on the upper part of the ROC plot. The optimum values are shown with respect to Youden index (J) and minimum distance to the optimum (d).

The results for the normalized SSI-CP for the testing data sets presented in Figure 4, refer to Classification 2, i.e. the data are classified according to load level. For the current analysis, the model order was chosen to be equal to 5, the block size was equal to 50 and the number of significant columns was equal to 15, while the confidence interval of the presented control charts was equal to 99% (a=1%). A better performance for the assumption of Gaussian distribution may be observed. In Figure 4(a) a few false detections are existent (i.e. beginning at load level 90%). Continuous damage detection takes place from the beginning of load level 120% until the end of the test (Figure 4(b)). Thus, the damage at the trailing edge and even the change of dynamic behavior due to fatigue were detected. The ROC in Figure 4(c) shows a very good overall performance and that the best performance was achieved for Classification 2 (Man2-dark blue curves).

In Figure 5 the results for the normalized VAR-CP (CP^{R^2}) are presented for the case of Classification 1 (Man1), which means that all data belong to one cluster. A model order equal to 35 and a confidence interval of 99% (a=1%) were chosen. Here, discrete distribution offers

a slightly better detection and there are no false detections. Continuous damage detection starts in the beginning of load level 130% until the end of the test. Also for this CP the best there is a very good overall performance and the best performance is achieved for Classification 2 (see ROC of Figure 5(c)).

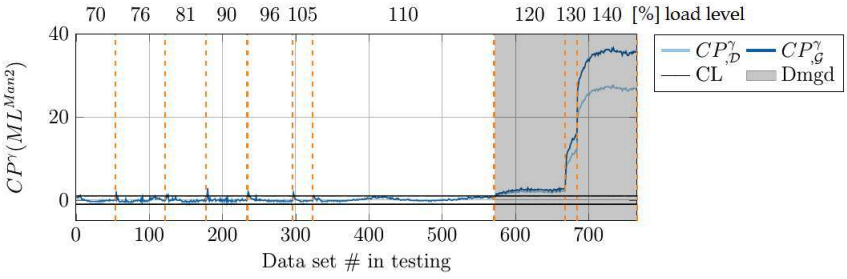

(a)

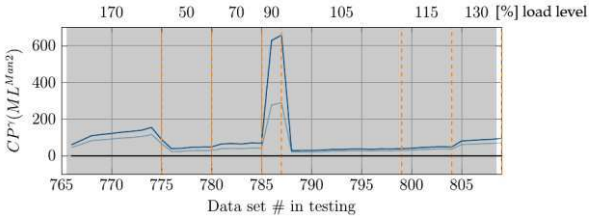

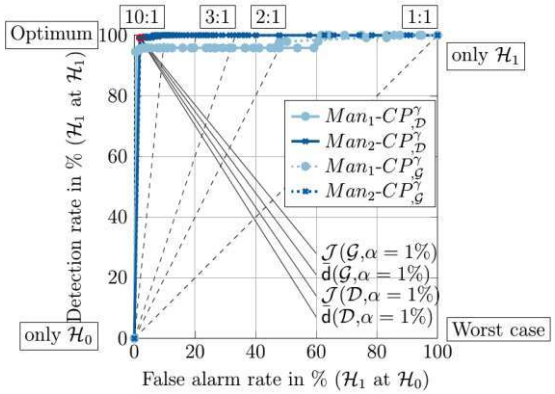

(b) (c)

Figure 4. Control charts for Classification 2 (a) and (b) and ROC curves (c) of the robust SSI Condition Parameter (CP^{γ}) - Load level in % shown on top of control charts.

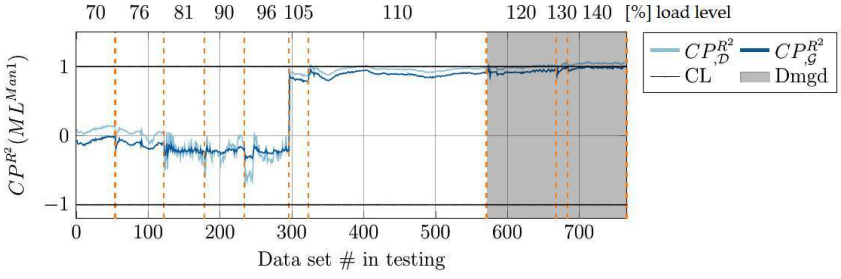

(a)

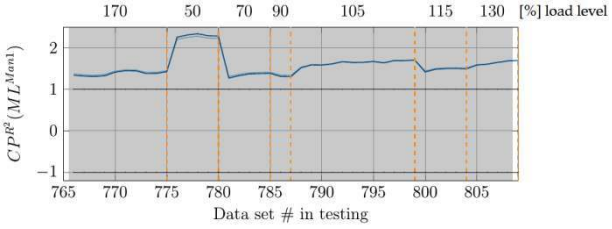

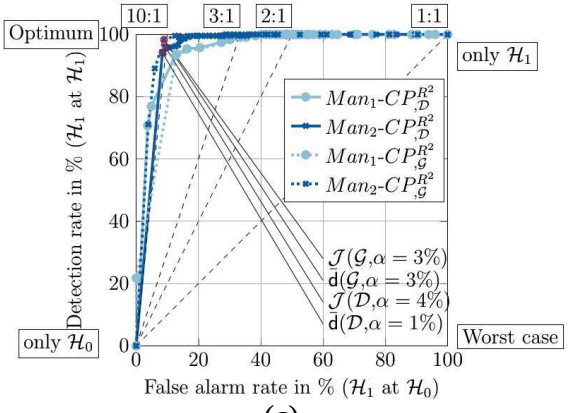

(b) (c)

Figure 5. Control charts for Classification 1 (a) and (b) and ROC curves (c) of the VAR Condition Parameter (CP^{R^2}) - Load level in % shown on top of control charts.

4.2 AIRBORNE SOUND DAMAGE DETECTION

During the fatigue test the three microphones recorded cracking sounds with different signal power. All these AEs were manually labeled and grouped by cracking sounds with high and low power. Only the high power sounds were found in all three microphone signals. The low power sounds are most likely connected with small damage events, but no valid mapping could be made with the damages found during the visual inspections. The cracking sounds with high power occurred only in test slots where relevant damage happened. The power of the two consecutive cracking sounds, which were emitted by the structural damage, is significantly greater than the power of the rest of the cracking sounds. The results of the labeling and the evaluation of the visual inspections support the assumption that the power of cracking sound signals can be used as an indicator for damage relevance. Prior to the structural damage in the same test slot, two further high power cracking sounds were found. These sounds might be caused by the structural damage in an early state. Three high power cracking sounds were observed during test slots in which the size of the structural damage increased. The results of labeling all cracking sounds can been found in Table 2. In Table 3 all high power sounds are listed.

Step # (Table 1)	1-8	9-10	11a	11b	12-14	15	16	17
# AE high power	0	0	0	4	0	1	0	2
# AE low power	7	3	16	84	1	3	0	14

Table 2: Occurrence of cracking sounds with high power and low power at all load steps.

Signal #	Step #	Description of the cracking sounds	f_{I1} [dB]	f_{I2} [dB]	f_{I3} [dB]
1	11b	55 min before the structural damage	-62.4	-72.5	-61.9
2	11b	1 min before the structural damage	-65.9	-78.1	-73.6
3	**11b**	**Structural damage**	**-42.9**	**-54.1**	**-51.4**
4	**11b**	**Structural damage**	**-48.8**	**-60.3**	**-55.8**
5	15	Crack propagation	-67.1	-74.1	-70.3
6	17	Crack propagation	-71.6	-80.3	-76.2
7	17	Crack propagation	-73.7	-76.8	-73.5

Table 3: Overview of all high power cracking sounds, f_I is the power of the sound of microphone one, two and three.

The airborne sound recordings of the whole fatigue test were processed by the AE damage detection algorithm. The threshold parameter of the power impulse feature was used to adjust the sensitivity of the damage detection performance. The structural damage was detected in all three microphone signals without false detections (Figure 6). If all high power cracking sounds need to be detected, the threshold of the power impulse feature is reduced. All these sounds were detected in microphone one with 144 false alarms. Damage detection of all high power events with simultaneous detections for all microphone signals is unfeasible due to the very high amount of false positive detections. In Figure 7 the corresponding part of the ROC curve is shown. The majority of the false alarms were made in test slot 11, in which the noise level is high due to the very high load level. This shows the limitations of the algorithm. If noise with very high power and similar impulse characteristic occurs, it is still possible to detect cracking sounds, which were

emitted by the crack propagation without false alarms but not in every microphone position. The results for detecting the structural damage are significantly better.

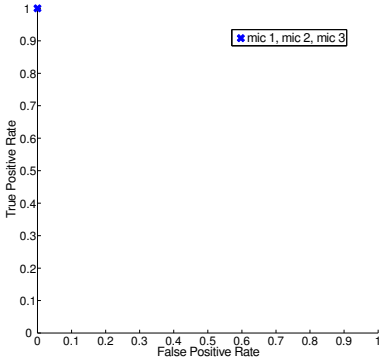

Figure 6. ROC of the airborne sound algorithm for detection of the two consecutive cracking sounds emitted by the structural damage.

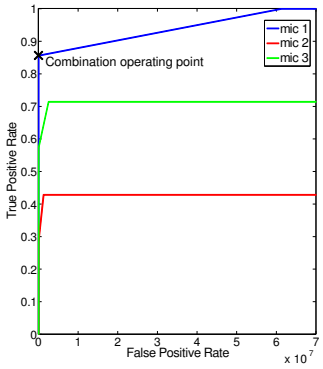

Figure 7. Part of the ROC curves for detection of all high power cracking sounds for microphone one, two and three, where no or a low amount of false positive detections were signaled.

5 COMBINATION OF THE TWO APPROACHES

One of the main goals of the current work was the combination of a vibration based SHM concept and an acoustic emission damage detection approach. For this purpose the databases of the two measurement systems were synchronized and the results were observed simultaneously. The two approaches have different sampling frequencies and damage intervals (10 minutes for the SHM-scheme and 5.3 milliseconds for the AE approch). Figures 8 and 9 present the synchronized damage detection of the two approaches: the SHM-scheme control chart and the accumulated AE detections. Figure 8 shows the damage detections for load levels 70% to 140% (undamaged and existence of fatigue signs). In Figure 9 the results are presented for the last part of the experiment (damage at the trailing edge and propagation).

On the left y-axis the control chart for CP^{R^2} (VAR-CP) for the case of discrete distribution and for a confidence interval equal to 99% is presented. On the right y-axis the airborne sound damage indicator is presented. The detections were here accumulated, so every detection adds one to the curve. A detection was derived by processing all microphone signals and giving a detection out if a cracking sound was detected in one of the three microphone signals. In these recordings no false positive detection were signaled for this procedure.

In the first part presented in Figure 8, the CP calculated by the SHM-scheme (CP^{R^2}) has no false detections and provides some detections in the second half of load levels 120% and 130% and continuous damage detection from the beginning of load level 140%. The acoustic system processed the recordings of the whole fatigue test and no detection during this first part were signaled (Figure 8). In the second part presented in Figure 9, CP^{R^2} continuously detects both damage occurrence and propagation as damaged states. The gaps contained in both figures correspond to data sets with intervals of test-start and test-stop or data sets that contained sensor mistakes, which were not included in the analysis. The AE system detects two events before the structural damage and the two consecutive emissions of the structural damage. Two additional detections are provided during load level 105% and 130%, where the damage propagation took place.

The conclusion can be drawn that the parallel observation and combination of the detection of the two damage approaches is beneficial, since the SHM scheme CPs provide information concerning the state of the blade (healthy or damaged) even for the case of structural changes due to fatigue, while the acoustic emission indicator provides information concerning damage events such as damage occurrence or propagation.

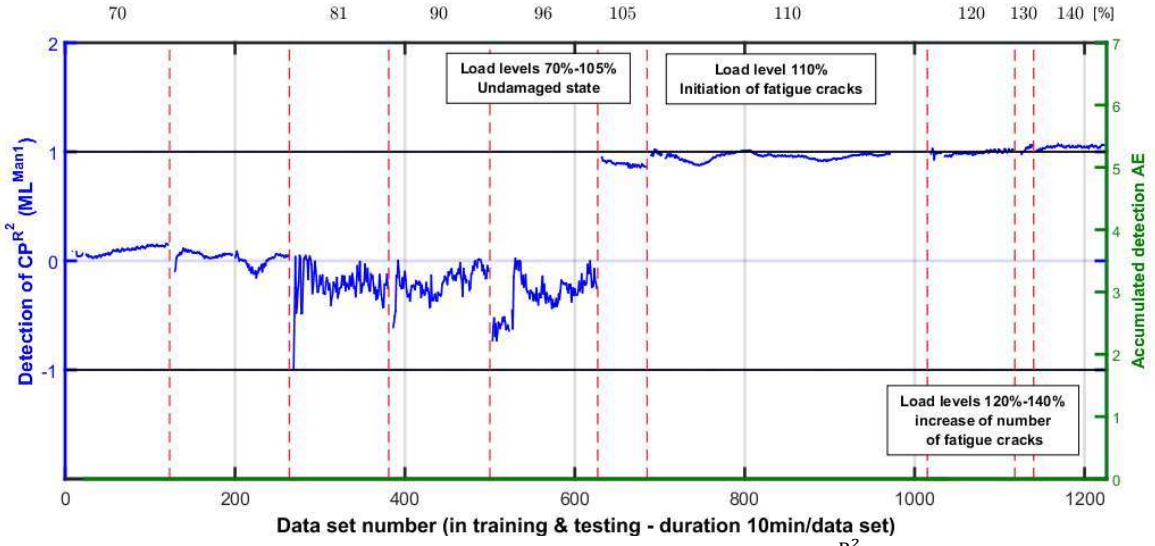

Figure 8. Comparison of the damage detection of the two approaches - CP^{R^2} of the SHM-scheme on the left y-axis and accumulated AE detections on the right y-axis (Part 1) - Load level in % shown on top.

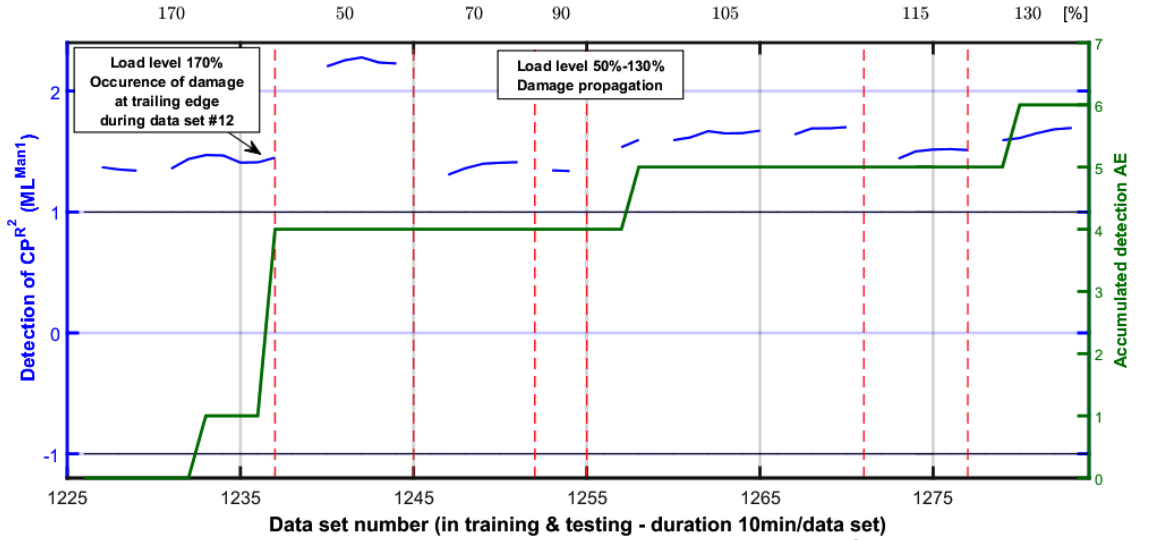

Figure 9. Comparison of the damage detection of the two approaches - CP^{R^2} of the SHM-scheme on the left y-axis and accumulated AE detection on the right y-axis (Part 2) - Load level in % shown on top.

6 CONCLUSIONS

The results of a SHM concept that consists of the three steps of machine learning, the calculation of CPs and hypothesis testing were compared to the results of an airborne sound damage detection algorithm for the fatigue test of a 34 m rotor blade. Four blade states were documented during the fatigue test: undamaged state, existence of fatigue, occurrence of a significant failure at the trailing edge and damage propagation.

For the SHM scheme, two CPs resulting from the SSI method and VAR models were presented for different settings, such as two types of classification, confidence intervals and assumptions for the CP distributions. Both provided detection of the damaged state of the blade for both cases of structural changes due to fatigue, damage occurrence at the trailing edge and propagation. The airborne sound damage detection algorithm detects the occurrence of the structural damage without a false detection. Events before the damage and events, where damage propagation took place, were detected without false alarms.

The observation of the results of the two approaches showed that the comparison and combination of different damage indicators derived from different methods and physical quantities can be beneficial for SHM. The two approaches function complementary, since the

CPs of the SHM-scheme provide information concerning the state of the blade (healthy or damaged), while the acoustic emission approach provides instantaneous information about damage events such as damage occurrence or propagation. Investigations for the application of both approaches under operating conditions belong to the future work of the authors.

7 REFERENCES

[1] D. Zarouchas, A. Antoniou, F. Sayer, D. Van Hemelrijck, and A. van Wingerde, "Structural Integrity Assessment of blade's subcomponents using Acoustic Emission Monitoring.," in Experimental and Applied Mechanics, Volume 6, T. Proulx, Ed. New York, NY: Springer New York, 2011, pp. 511–518.

[2] A. Ghoshal, M. J. Sundaresan, M. J. Schulz, and P. Frank Pai, "Structural health monitoring techniques for wind turbine blades," J. Wind Eng. Ind. Aerodyn., vol. 85, no. 3, pp. 309–324, Apr. 2000.

[3] S. Zerbst, S. Tsiapoki, and R. Rolfes, "Novel approach for early damage detection on rotor blades of wind energy converters," Smart Struct. Syst., vol. 14, no. 3, pp. 419–444, Sep. 2014.

[4] C. Boller, F.-K. Chang, and Y. Fujino, Encyclopedia of structural health monitoring. Chichester, West Sussex, U.K.: John Wiley, 2009.

[5] S. G. Taylor, G. Park, K. M. Farinholt, and M. D. Todd, "Fatigue crack detection performance comparison in a composite wind turbine rotor blade," Struct. Health Monit., vol. 12, no. 3, pp. 252–262, May 2013.

[6] M. W. Häckell, "A Holistic Evaluation Concept for Long-Term Structural Health Monitoring," Dissertation, Leibniz Universität Hannover, Fakultät für Bauingenieurwesen, Institut für Statik und Dynamik, Hannover, Germany, 2015.

[7] M. W. Häckell and R. Rolfes, "Monitoring a 5MW offshore wind energy converter. Condition parameters and triangulation based extraction of modal parameters," Mech. Syst. Signal Process., vol. 40, no. 1, pp. 322–343, Oct. 2013.

[8] M. W. Häckell, R. Rolfes, J. P. Lynch, and M. Kane, "Three-Tier Modular Structural Health Monitoring Framework Using Environmental and Operational Condition Clustering for Data Normalization: Validation on an Operational Wind Tirbine System," no. Proceedings of the IEEE, accepted on May 2016.

[9] S. Tsiapoki, M. W. Häckell, and R. Rolfes, "Monitoring of a 34 m wind turbine rotor blade during a fatigue test by a modular SHM-Scheme," in 10th International Workshop on Structural Health Monitoring, IWSHM 2015, Stanford, CA, USA, 2015.

[10] T. Krause, S. Preihs, and J. Ostermann, "Acoustic Emission Damage Detection for Wind Turbine Rotor Blades Using Airborne Sound," in 10th International Workshop on Structural Health Monitoring, IWSHM 2015, Stanford, CA, USA, 2015.

[11] T. Krause, S. Preihs, and J. Ostermann, "Airborne Sound Based Damage Detection for Wind Turbine Rotor Blades Using Impulse Detection in Frequency Bands," in 1st International Wind Engineering Conference, Hannover, Germany, 2014.

[12] T. Krause, S. Preihs, and J. Ostermann, "Detection of Impulse-Like Airborne Sound for Damage Identification in Wind Turbine Rotor Blades," in 7th European Workshop on Structural Health Monitoring, EWSHM 2014, Nantes, France, 2014.

[13] M. Basseville, L. Mevel, and M. Goursat, "Statistical model-based damage detection and localization: subspace-based residuals and damage-to-noise sensitivity ratios," J. Sound Vib., vol. 275, no. 3–5, pp. 769–794, Aug. 2004.

[14] M. Döhler, L. Mevel, and F. Hille, "Subspace-based damage detection under changes in the ambient excitation statistics," Mech. Syst. Signal Process., vol. 45, no. 1, pp. 207–224, Mar. 2014.

[15] J. Neter, W. Wasserman, and M. H. Kutner, Applied linear statistic models, vol. 4. Irwin Chivago, 1996.